Geomechanical Modeling of Mining-Induced Permeability: Implications for Potential Gas Inflow from a Sheared Gas Well

Z. Khademian
K.M. Ajayi
D.W.H. Su
G. Esterhuizen
S.J. Schatzel
National Institute for Occupational Safety and Health,
Pittsburgh Mining Research Division, Mining Systems and Safety Branch

ABSTRACT

Stability and integrity of unconventional shale gas wells drilled through current and future coal reserves can be compromised by ground deformations induced by nearby longwall mining operations. Due to the enhancement of the surrounding rockmass permeability by longwall mining, the high-pressure gas from a damaged, breached well may reach mine workings and overwhelm ventilation system capability to dilute the hazardous atmosphere. This paper describes a set of in-situ measurements coupled with a modeling procedure that uses geomechanical analyses for estimating longwall-induced rockmass permeability and estimates potential inflow to the mining area by a fracture flow analysis. A two-panel longwall model is constructed to represent a shallow 147 m-deep mining site in the southwestern Pennsylvania coal region. A Distinct Element Code (3DEC) is used to explicitly model the rockmass by a Discrete Fracture Network (DFN) logic. Field observation, surface subsidence measurement, underground coal pillar stress measurements, and in-situ permeability measurements are used for calibrating DFN geometries and initial aperture values. The fracture aperture distribution across the model is used for predicting potential shale gas inflow to the mine using a Fracture Flow Code (FFC) developed for this study. Several realizations are simulated to cover worst-case scenarios for the maximum inflow into the mining area in a comparative analysis. The presented modeling approach will help investigate the potential hazards of a shale gas well for mine safety should the well casing integrity be compromised by mining operations.

INTRODUCTION

In the Northern Appalachian Basin of the US, most of the shale gas production wells into unconventional shale gas reservoirs intersect with a bedded sequence of minable coal layers. Since 2011, about 2400 drilling permits have been issued every year for unconventional shale gas reservoirs by the Pennsylvania Department of Environmental Protection (PADEP 2018). Longwall mining of the Pittsburgh coal bed will mine by many unconventional gas wells in the Marcellus shale within the next five years.

Active or future longwall operations can coexist with shale gas production but require specific design considerations for ensuring the safety of both operations. One of the main safety hazards can be the gas wells whose integrity could be compromised by longwall-induced deformation, leading to flow of explosive high-pressure gas into the mining area. The current design regulation for protecting gas wells from the effects of mining follows the 1957 Pennsylvania gas well pillar study (Commonwealth of Pennsylvania 1957), which has been widely used by the Mine Safety and Health Administration (MSHA) and by other states over the last 60 years to address gas well pillar stability issues. However, the advancement in the unconventional gas resource development and mining technologies have led to an increased number of gas wells drilled into mining areas with elevated mining rates under deeper cover and thus demand revisiting the current design regulations.

In 2012, the PADEP initiated a call for research to update the gas well pillar regulations. To provide scientific input towards this effort, the National Institute for Occupational Safety and Health (NIOSH) initiated an ongoing research project starting in 2017 to 1) evaluate the effects of strata deformations on the stability of shale gas casings; 2) estimate longwall-induced permeability changes in the ground; and 3) analyze possible inflow into the mining area in the case of a gas well breach. Initial findings from this project identified that one of the possible horizons for potential well casing failure is at the Sewickley horizon above the Pittsburgh coal bed (Su et al. 2019; Zhang et al. 2020). Following this finding, NIOSH is investigating the possible effects of a hypothetical casing failure in this location on gas inflow into the mining area by estimating rockmass permeability.

Fluid flow within a fractured rock is mostly affected by the rockmass permeability that can be enhanced by the mining-induced stress and subsurface movement. Quantitative analyses of potential inflow need an understanding of the rockmass permeability, especially in the proximity of the mining activities and the well location. Relevant field permeability measurements are extremely challenging because of the number of required measurement points

and scale of testing to fully capture the mining-induced permeability evolution over time. Laboratory experiments can also provide limited information on small-scale fracture permeability distribution. Numerical modeling is a practical alternative, but modeling rockmass permeability also remains as a challenge in rock mechanics because of the difficulty in accessing and replicating the exact fracture network in the overburden rock. One approach is to use stochastic modeling techniques such as DFN for generating fracture networks and then calibrating their geometries using field measurements. Due to the number of unknown parameters and the nature of stochastic analyses, such a process is not unique, so the calibrated model may represent only one of the possible realizations that can reproduce the field measurements. This issue can be partially addressed by using the calibrated fracture properties as the basis for a set of stochastic analyses that provide a range of possible outcomes.

The approach outlined in this paper uses geomechanical analyses informed by in-situ measurements for limiting and calibrating the DFN parameters. The calibrated parameters, such as the aperture of fractures, is then used to construct a stochastic DFN flow model. After ensuring the stochastic calculation of permeability in 100 realizations remains within the range of field measurements, we compute the range of gas inflow volumes traveling through the rockmass to the mining area in the case of a sheared gas well.

METHODOLOGY

This study includes a series of in-situ measurements and numerical model analyses to comparatively investigate the range of potential influx to the mining area from a damaged gas well drilled into a longwall abutment pillar. The study is conducted in the Northern Appalachian Basin in a longwall mine in the Pittsburgh coal bed. Gama ray, resistivity logging, and field observations are used to construct a geomechanical model and a Fracture Flow Code (FFC) model based on a DFN approach. An in-seam installed Borehole Pressure Cell (BPC) study, surface subsidence surveys, and in-situ rockmass permeability measurements are conducted for calibrating and validating the models. Fracture apertures obtained from the calibrated geomechanical model are exported to the FFC model, which has the capability of simulating numerous DFN realizations with manageable runtime, for estimating the possible range of gas inflow into the mining area in the case of a breached gas well.

In-Situ Measurements

The study was conducted in a longwall mine in the Pittsburgh coal bed. Overburden geology to the mining depth of 147 m was interpreted by correlating a test site gamma log and a nearby core hole, demonstrating many strong-to-weak rock interfaces (Su et al. 2019). The weak Uniontown coal horizon at the approximate depth of 76 to 81 m and the Sewickley coal horizon at 119 to 126 m indicate potential planes of weakness that can be significantly affected by the longwall-induced deformation.

Figure 1 shows a plan view of the study site with a 33-m by 79-m abutment pillar that is part of a three-entry longwall gate road system. Four Borehole Pressure Cells (BPC) were installed into the abutment pillar along with a pre- and post-longwall surface subsidence surveys. The first and second panels approached and mined by the test site in July 2018 and May 2019, respectively. Surface subsidence surveys were conducted when the first panel longwall face was about 220 meters inby the test site and when the first panel longwall face was 920 meters outby the test site. After the second panel mined by the test site, the subsidence was again measured in June 2019.

Four monitoring boreholes were drilled in the overburden directly above the abutment pillar between two planned longwall panels. Three of the four monitoring boreholes, labeled as FEB1, FEB2, and FEB3 in Figure 1, were used for slug permeability tests as the first and second panels mined by the test site. FEB1 had a depth of 127 m, FEB2 had a depth of 76 m, and FEB3 had a depth of 41 m. The FEB1, FEB2, and FEB3 boreholes were cased and cemented,

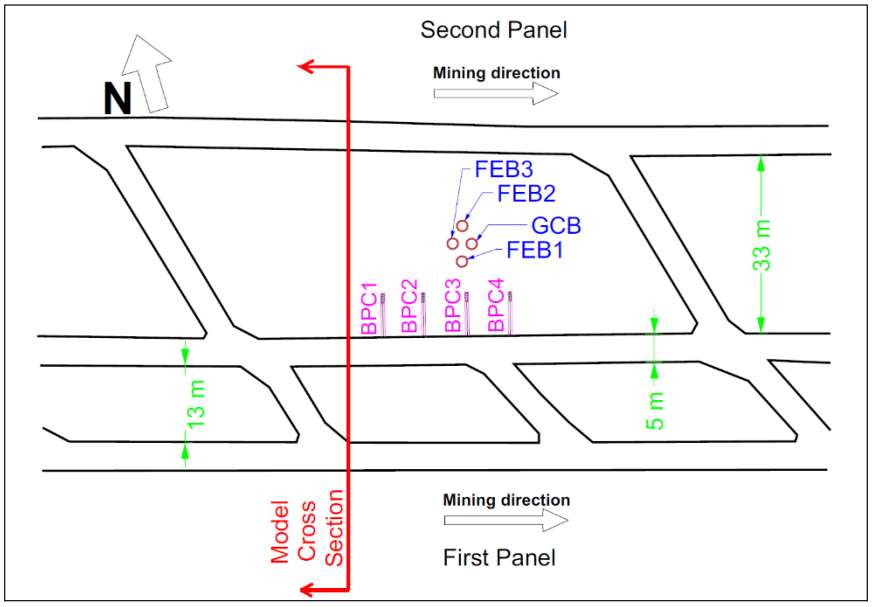

Figure 1. Plan view of the instrumentation layout and three-entry gate road system

except for the bottomhole test intervals of 8 m, 2.5 m, and 2 m, encountered by Waynesburg, Sewickley, and Uniontown horizons, respectively (Watkins 2020).

The fourth borehole, shown as GCB in Figure 1, was for installing inclinometer sensors oriented along the direction of longwall mining to capture the influence of the east-west regional horizontal stresses. So, the ground movements measured by the inclinometer are directed out of the plane of the pseudo-2D model cross section shown in Figure 1 and could not be used to verify the accuracy of the model.

Geomechanical Model

A three-dimensional distinct element code, 3DEC, is used for constructing a pseudo-2D longwall model of the study site (Figure 1) with one-meter length in the out-of-plane direction. From the core log data, 50 geologic layers are modeled each with a thickness greater than 0.6 m (Figure 2). The model length is extended in the *x* direction to a total of 9,000 m to avoid any boundary effects. The rock types in the overburden are shale, sandstone, sandy shale, limestone, coal, and shaley limestone with field-scale geomechanical properties listed in Table 1.

Given the purpose of this study, DFN is used for explicitly modeling fractures in rockmass since the fluid flow through fractures vastly dominates the flow through matrix pores. This is because the cross-sectional area, and thus the flow rate through fractures, is several orders of magnitude larger than that of pores within the intact rock.

Table 1. Geomechanical properties applied to the model for each lithology

Rock Type	E (GPa)	ν	C (MPa)	φ°	T (MPa)
Coal	1.72	0.3	6.21	28	0.28
Shale	11.58	0.25	11.72	35	4.50
Sandy Shale	11.58	0.25	11.72	35	4.50
Sandstone	11.58	0.22	17.93	35	6.88
Shaley limestone	17.37	0.22	14.48	38	5.93
Limestone	17.37	0.25	15.93	35	6.12

E: Elastic Modulus, ν: Poisson Ratio, C: Cohesion, φ: internal Friction Angle, T: Tension

In the next two sections, the techniques for modeling fractured rock and fracture permeability calculations are discussed. The process for calibrating mechanical and hydraulic fracture properties are also explained.

Modeling Fractured Rock

One of the challenges in DFN implementation for simulating fractured rock is limiting site-specific fracture geometry and frictional properties that best represent rockmass behaviors under stress. Fracture geometry is defined as the distribution of fracture orientation, length, and density. Observation from longwall-induced fracture orientations suggests propagation of high-angled fractures perpendicular to the mining face. Thus, the DFNs are modeled with a constant dip direction of 90 degrees (perpendicular to the face) and a dip angle with a mean of 90 degrees that is defined using a Von-Mises Fisher's distribution (Best and Fisher 1979). The dip angle variance is approximated to be 15° from 0–10 m above the mine roof, 12° from 10–30 m, 10° from 30–60 m, and 5° degree for the rest of the domain, derived from field observation in Southwest Pennsylvania (Kohl 1980).

The length of fractures is assumed limited to the thickness of host strata with a negative power law distribution with a scaling exponent of 1.1. Uniform distribution is used for the fracture position within each individual lithology because fracture systems are mostly affected by the physical properties of the host rock (Feng et al. 2018).

The fracture density is defined as the P32 value, which is the cumulated fracture surface in the specified region per unit volume. For this specific site, no data was collected on the fracture density, so the values are calibrated using the field measurements during the completion of the **first** panel. The initial values for the calibration are derived from fracture density measurements reported in a study in Tahmoor Colliery (New South Wales, Australia) across

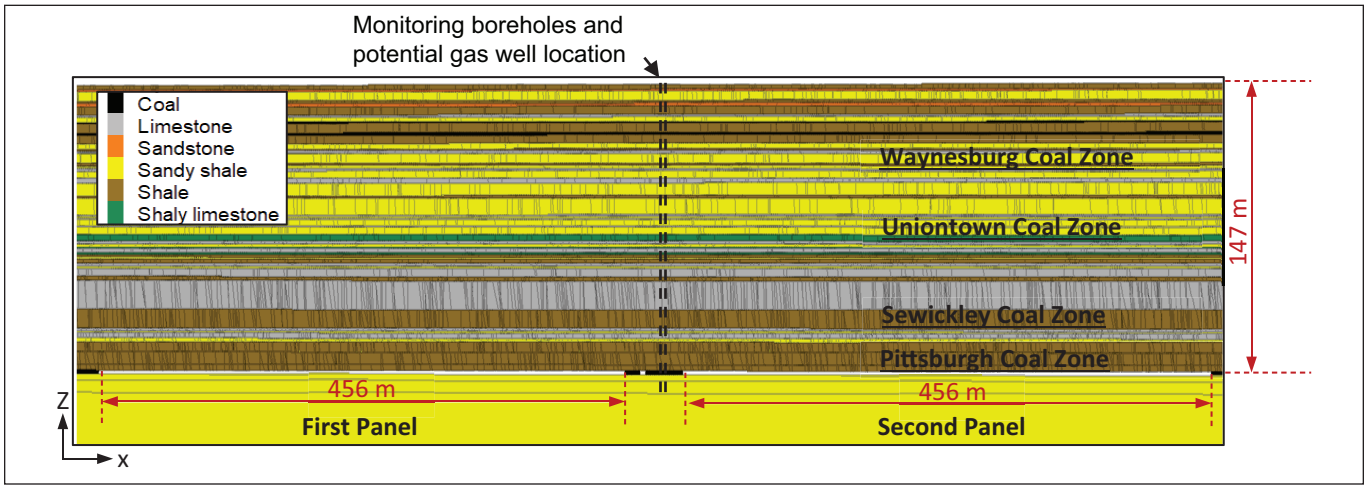

Figure 2. Detail of the central part of a 3DEC model of a shallow longwall mine with DFN elements defining rockmass structures in 50 modeled lithologies

a 424-m mining depth (Holla and Buizen 1991). Fracture densities are limited to a 0.1 to 0.3 m^2/m^3 range with higher densities applied to weaker zones that are defined by the logging data and field observations. The weak zones include the shallow weathered zone, Waynesburg horizon, Uniontown horizon, Sewickley horizon, and an interconnected fracture zone. The combined thickness of the caved area and the lower part of the fractured zone above it is defined as the interconnected fracture zone that represents a system of channels allowing flow transport to the mine level. Through a set of field measurements, (Palchik 2003) suggested that the interconnected fracture zone is within the 19–43 times the mining height.

The friction coefficients of fractures can vary within a range of 10 to 25 degrees suggested for fault gouge and smooth rock surfaces, respectively (Iannacchione 1990). Friction coefficients of fracturs in each geologic layer are calibrated using the field measurements during the completion of the **first** panel. The fracture friction is varied as a percentage of the rock internal friction for each layer (Table 1) as long as it still remains within the range of 10 to 25 degrees. However, a constant friction angle is assigned to the DFNs in the interconnected fracture zone in all cases.

The effects of gob materials on the mining-induced deformations should also be considered for making modeling results and field measurements comparable. The compaction of the gob and residual voids in the gob are accounted for by limiting the vertical displacement of the roof to between 70% and 85% of the mining height. Finally, the calibrated DFN properties are shown to represent the study site by comparing modeling results with the field measurement during the completion of the **second** panel.

Rockmass Permeability

As discussed, rockmass permeability is mostly governed by the permeability of fractures; thus, we assume the rock matrix permeability is zero. According to the cubic law in Equation 1, the laminar flow rate through fractures is exponentially related to the fracture aperture (b), which is a function of the physical distance between fracture plates and fracture roughness.

$$Q = -\frac{\rho g\, b^3\, w}{12\,\mu\, L}\,\Delta H \tag{1}$$

In Equation. 1, Q is the volume flow rate (m^3/s), ΔH is the pressure head difference (m), ρ is the density of fluid (kg/m^3), L is the length of the fractures (m), b is the fracture aperture (m), g is the acceleration due to gravity (m/s^2), μ is the dynamic viscosity of methane in air (Ns/m^2), and w is the fracture height or out-of-plane length of the fracture (m). In this geomechanical model, b is estimated from an initial aperture value and the fracture deformation computed by stress analyses, given as:

$$b = b_0 + F \cdot u \tag{2}$$

where F is a correction factor relating to the fracture roughness and flow tortuosity, b_0 is the **initial** aperture value **before** stress analyses, and Δu is the fracture deformation **after** applying mechanical stresses. In the geomechanical model, Δu can be calculated through the relationship between stress, displacement, and constitutive laws, but b_0 and F are unknown variables and depend on the fracture slip history and intrinsic roughness. This paper assumes fractures have smooth surfaces, and thus F is assumed to be one but b_0 is obtained through a calibration process using pre-mining permeability measurements before the first panel is mined by the test site. To this end, we assign a constant b_0 to all DFNs and bedding planes in the model before initiating in-situ stresses. When the model is solved under in-situ stresses, some fractures are activated, and their fracture apertures evolve based on the dominant stress regime. The permeability of each layer is calculated and compared against the measured values. This process is repeated until the modeled permeability of fractures approaches those of pre-mining slug test results.

The fracture permeability calculation follows a method described in (Zhang et al. 1996). Referring to the Cubic Law in Equation 1 and Darcy's equation, permeabilities are related to the pressure head gradients and flow rate as:

$$\begin{bmatrix} q_{xx} & q_{xz} \\ q_{zx} & q_{zz} \end{bmatrix} = \begin{bmatrix} K_{xx} & K_{xz} \\ K_{zx} & K_{zz} \end{bmatrix} \begin{bmatrix} \nabla H_x & 0 \\ 0 & \nabla H_z \end{bmatrix} \tag{3}$$

where q indicates the direction and velocity (m/s) of flow and is the sum of boundary flow Q divided by the boundary area. ∇H_x and ∇H_z are the dimensionless pressure head gradients in the x and z directions, respectively. K is the permeability coefficient or conductivity (m/s).

The constructed model can simulate flow in all fractures irrespective of their orientation but estimates the permeability of each stratigraphic layer by assuming that the near-vertical fractures have the dominant role in the overall permeability of the layer. Therefore, each layer is isolated in the model, and a pressure head is applied onto the top and bottom of the layer limited to the area above the pillars. Flow through high-angled fractures q_{zz} are then recorded, and the permeability coefficient in Equation 3 is calculated. The corresponding intrinsic or absolute permeability (m^2) is then obtained from:

$$k = \frac{K\mu}{\rho g} \tag{4}$$

The calculated permeability is limited to the area above the pillar. This makes the results more comparable with the values measured from the slug test, which was conducted in the FEB boreholes drilled above the abutment pillar.

Fracture Flow Code (FFC) model

Once the mechanical and hydraulic fracture properties are calibrated in the geomechanical model, the range of potential inflow to the mining area can be calculated. Based on the complexity of this problem, there are limited commercial software programs that can simulate the details intended for modeling with a manageable computation time, which is required for stochastic analyses. NIOSH researchers developed the FFC model that is based on the DFN scheme to calculate potential flow to the mine in the event of a breach. The flow through the fractures is solved using the cubic law in Equation 1. The fracture nodes are classified as external and internal nodes with the assumptions of known pressure head at the external nodes or boundaries. By applying mass conservation at the internal nodes, an algebraic set of equations are formed and solved to obtain the pressure head of internal nodes. The internal node pressure head closest to the mine horizon is used to calculate the potential flow to the mine. Figure 3 shows the model configuration in the FFC.

Similar to the geomechanical model in 3DEC, 50 layers are modeled with a thickness greater than 0.6 m, and the vertical fractures

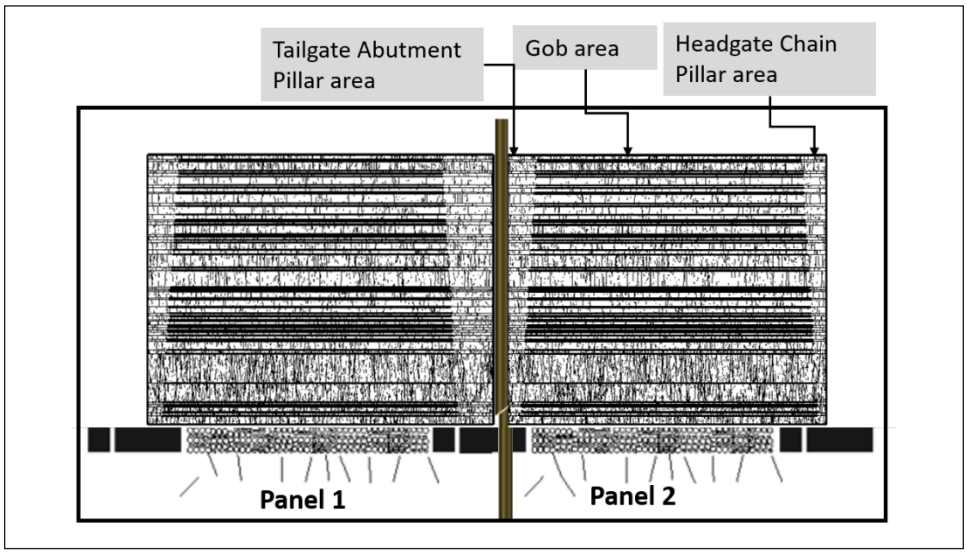

Figure 3. FCC model configuration with three areas defined to apply the variability of the 3DEC aperture values.

are modeled with a similar fracture density function. DFN location and orientation distributions also follow the geomechanical model. However, the fracture apertures follow a lognormal distribution with the peak values obtained from the geomechanical model. Applying a lognormal distribution to the aperture values allows for a stochastic analysis on the variation of apertures and their effects on the possible range of inflow to the mine. Aperture values are also modified to account for the fracture water saturation effects on the inflow calculation.

In previous studies by (Kissell and Edwards 1975) on two-phase flow in coalbeds, they observed that methane emission is increased as the fracture water saturation level decreases, indicating the effect of relative permeability. So, the gas permeability increases as the water content of the coal decreases. Based on this observation, (Kissell and Edwards 1975) assumed an initial water saturation of over 70% for the simulation. Hence, it is well established that fractures in the Northern Appalachian basin are saturated with water to some extent. In order to model a potentially worst case for gas transport, we assume that the fractures are saturated with stationary water up to 25%. This implies that 75% of the aperture opening is available for gas flow.

After constructing the FFC model, the analysis is conducted for a breach of an operating gas well at the Sewickley horizon. An operating gas pressure head of 2.4 MPa (350 psi) is defined at 23 m above the mine level at the center of the abutment pillar. The pressure at the mine level is set to –1,500 Pa representing the ventilation system and the shale gas is modeled as methane.

RESULTS

Geomechanical Model Calibration and Validation

The measured pillar stress and surface subsidence after the first panel mined by the test site are used for calibrating DFN density, fracture friction, and gob effects in the model. Thus, the calibration process starts by a systematic variation of the fracture density, fracture friction, and gob deformation. Next, the pre-mining permeability measurement is used for calibrating the initial aperture

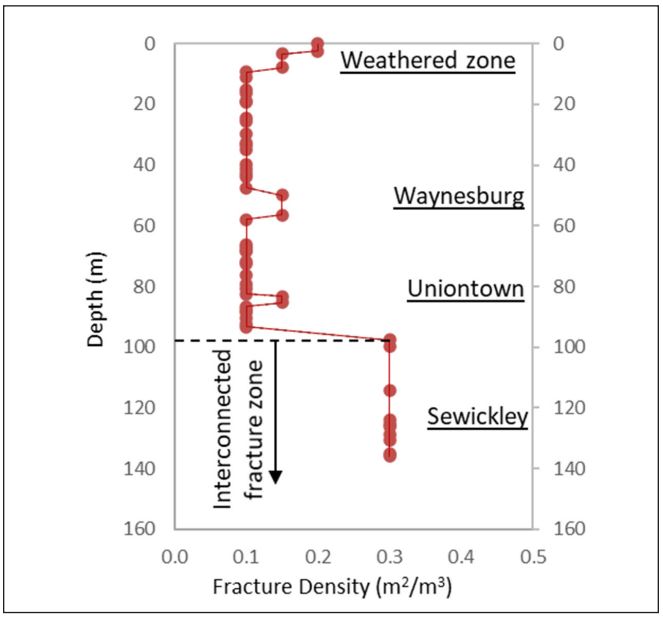

Figure 4. DFN density applied to generate high-angled fractures

value b_0. The results show that with a roof maximum displacement of 70% of the mining height, the fracture friction of 60% of the rock internal friction, and fracture density pattern shown in Figure 4, the pillar stress (Figure 5) and subsidence measurements (Figure 6a) fall within the range of measured data. Higher fracture densities are assigned to the weaker zones (Figure 4). The interconnected fracture zone is defined with a height 23 times the mining height. The friction of both DFN and bedding planes are 60% of the internal friction of rock in each layer, except for the layers within the interconnected fracture zone where a constant friction angle of 10 degrees is assigned to the DFNs.

Figure 5 compares the measured and computed pillar pressure after the completion of the first panel. Figure 6a compares the modeled

and measured subsidence records after the first panel is mined. The measured and computed maximum supercritical subsidence are 1.38 meters or 0.67 times the 2.07-m extraction height.

In the next step, permeability measurements are used to calibrate b_0 the initial aperture assigned to the fractures in the model. The results show that an initial aperture of 0.5 mm gives the relative agreement between the pre-mining values of permeability from site measurements and from 3DEC in Figure 7a. The maximum value of permeability recorded during the slug test is considered for this process.

Once the model is calibrated, the second panel is simulated and results are compared with the subsidence records (Figure 6b) and permeability measurements (Figure 7b and Figure 7c) when the second panel mined by the test site. At the Sewickley horizon, the maximum permeability measured during the field study was 1.4 Darcy for panel 1 and 5.1 Darcy for panel 2. Since the first panel was completed before the second panel, the combined impact of mining both panels is measured during the second panel mining. The relative agreement between the modeled and measured values validates the calibration process and allows for further analyzing the gas flow through the fractured rock using the calibrated DFN geometry and fracture apertures.

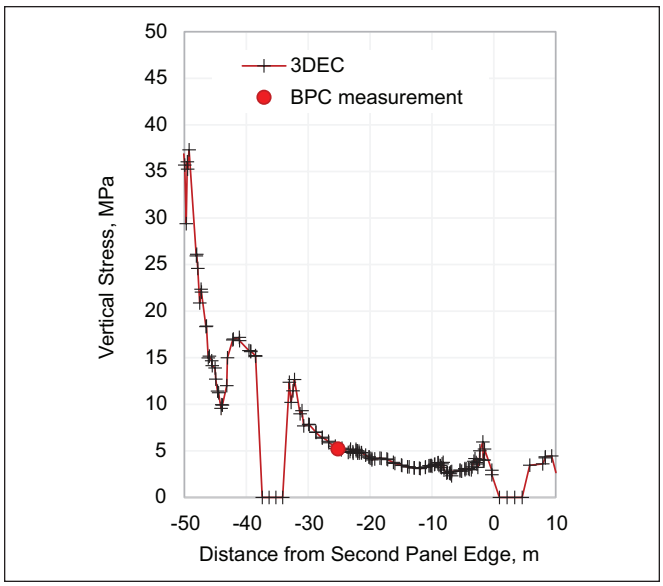

Figure 5. Comparison between the pillar stress measured by BPC and 3DEC calculation results

Aperture Variation

The geomechanical model outputs that are useful for gas flow analyses in FFC are DFN geometry and fracture apertures. Figure 8a and Figure 8b show the aperture of DFN and bedding plans, respectively, above the abutment pillar over the entire depth of overburden. The mechanism behind the wide variation of aperture values can be understood from the aperture contours outlined in Figure 9.

Aperture values above 1 mm in Figure 8a are mostly related to the DFNs above the panel edge (Figure 9) where strata curvature and bending occurs as a result of a high concentration of shear and tensile stresses which activates nearby fractures and enhances their aperture values. The lower values of aperture are associated with the DFNs above the caved zone at the center of the panels. This can be related to the re-compaction of the overburden after mining and the absence of curvature of the settled strata.

In Figure 8b, the aperture values above 1 mm are mostly associated with the bedding plane separation at the panel edges and the caved zone (Figure 9). A lower range of aperture values in Figure 8a is related to the high vertical compression from the overburden loads mostly concentrated above the pillars and the region above the gob at the center of the panels. Using the computed fracture apertures, flow analyses can be perfomed to estimate potential inflow of gas from a sheared gas well to the mining area.

3DEC includes a built-in fracture flow analysis that explicitly solves flow through fractures using a time-marching scheme. However, the wide range of aperture values shown in Figure 9

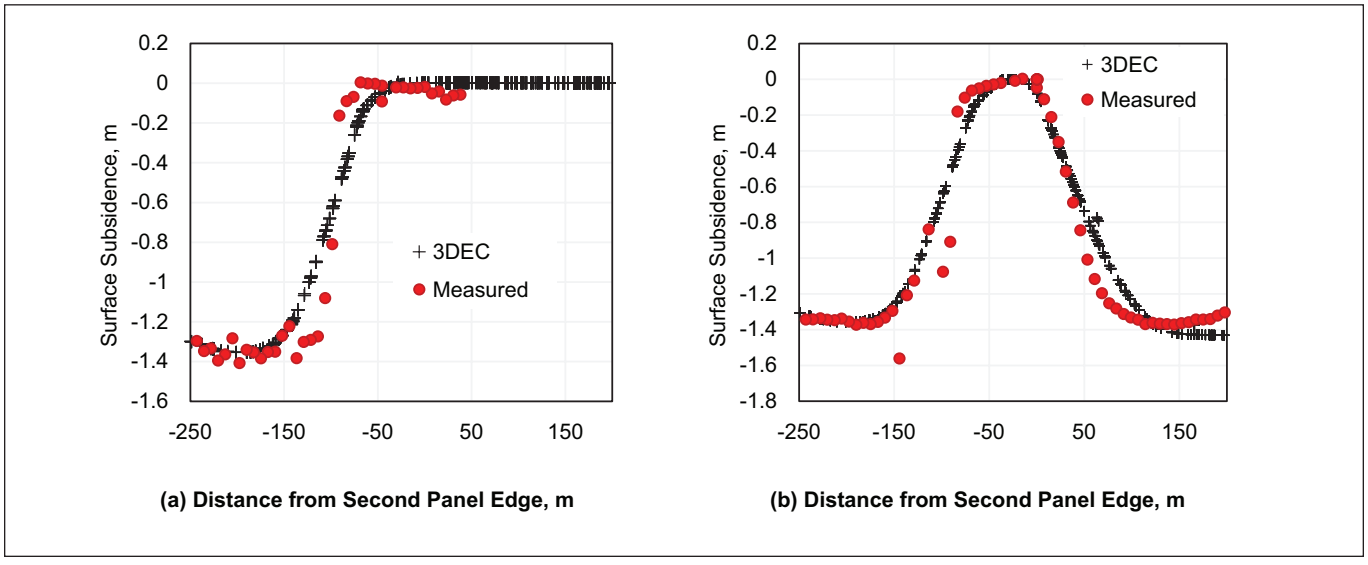

Figure 6. Modeled and measured surface subsidence (a) after mining the first panel and (b) after mining the second panel.

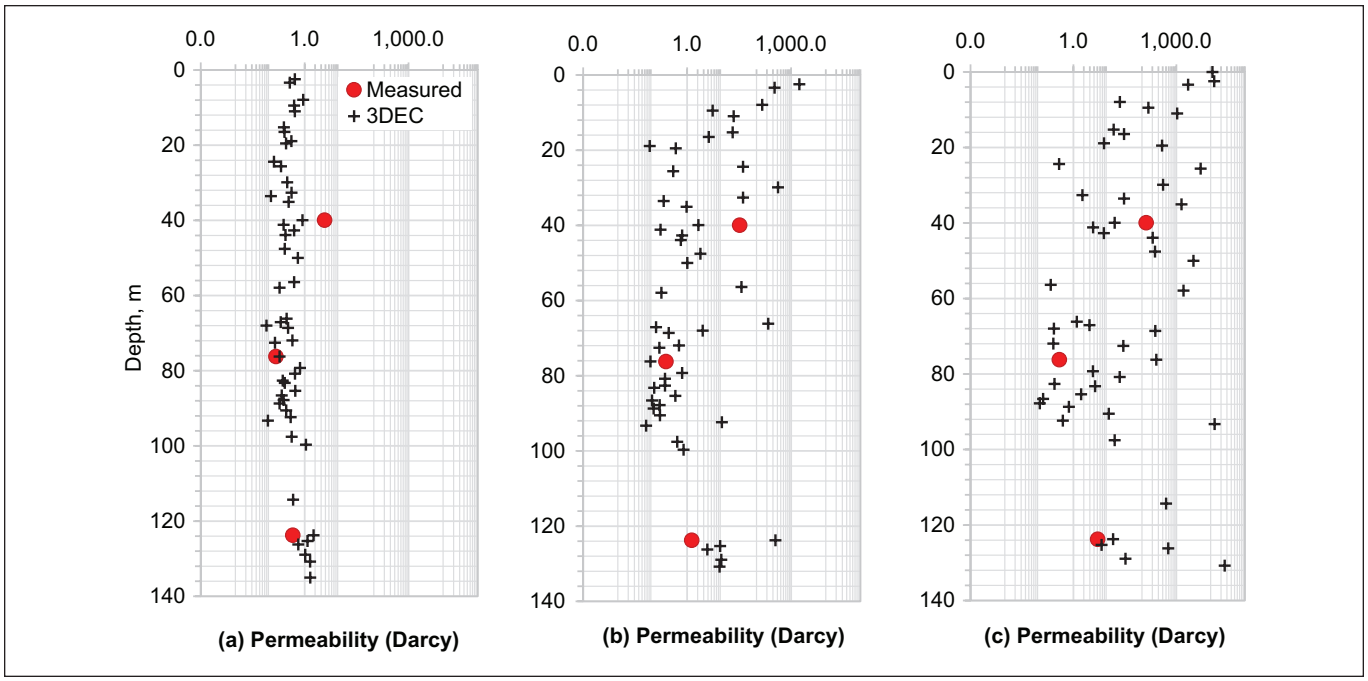

Figure 7. Results of computed and measured permeability along the depth for (a) first panel mining face is inby the test site, (b) first panel mining face is outby the test site, (c) second panel is outby the test site.

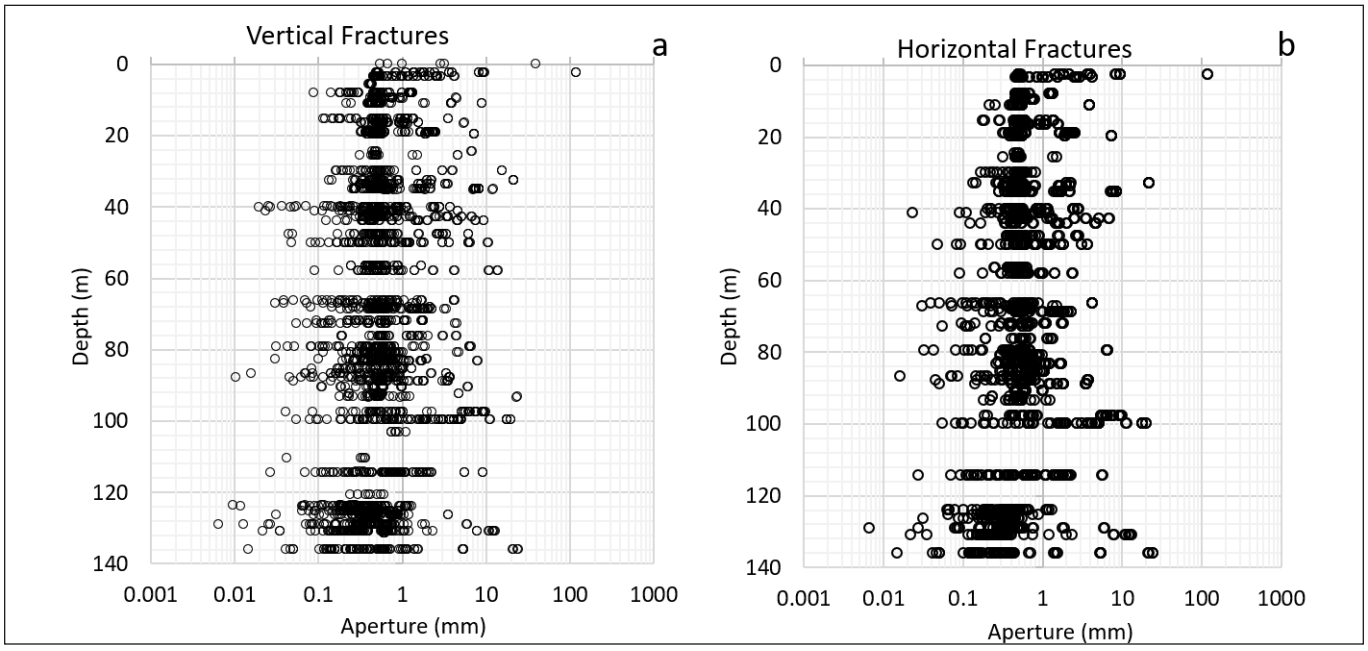

Figure 8. 3DEC results on the aperture values for (a) DFN fractures and (b) bedding planes over the abutment pillar

enforces a small timestep that significantly increases the runtime and thus prevents a stochastic analysis of inflow. For this reason, the spatial distribution of aperture data is incorporated into the FFC that is developed based on an implicit approach enabling extensive analyses on potential range of inflow to the mining area with significantly reduced runtimes. To provide confidence on the functionality of the FFC model, a simple case of fracture flow with constant aperture values is constructed in both 3DEC and FFC, and the results are compared in the next section.

FFC Model Validation

In an effort to verify the inflow results from the FFC model, a simplified single zone model was developed in both 3DEC and FFC. Given the objective, a small fracture aperture is assumed and

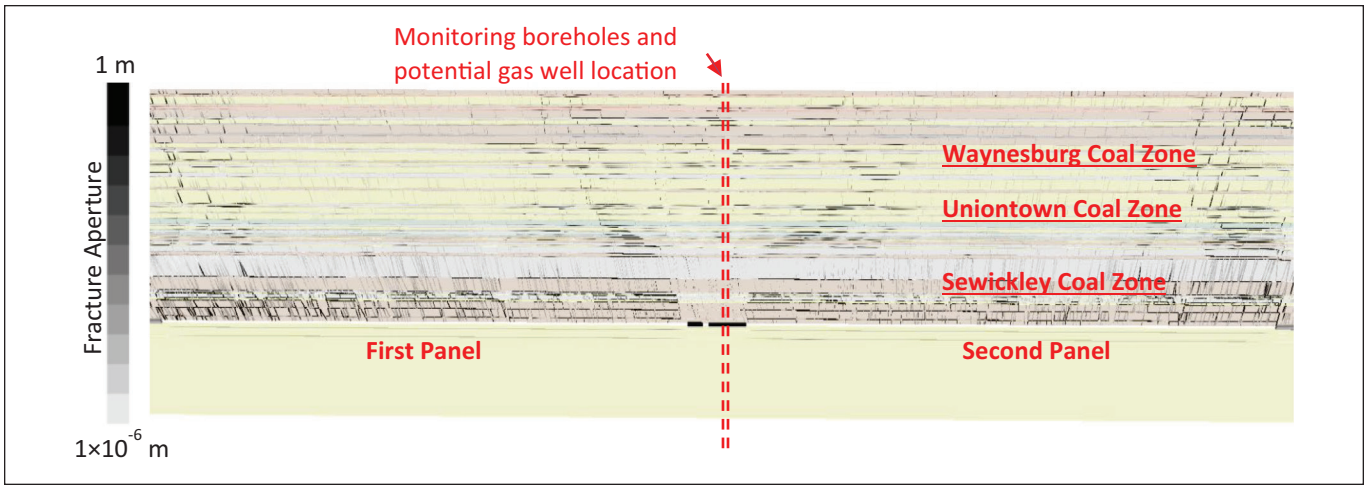

Figure 9. Fracture aperture contours after the second panel is mined.

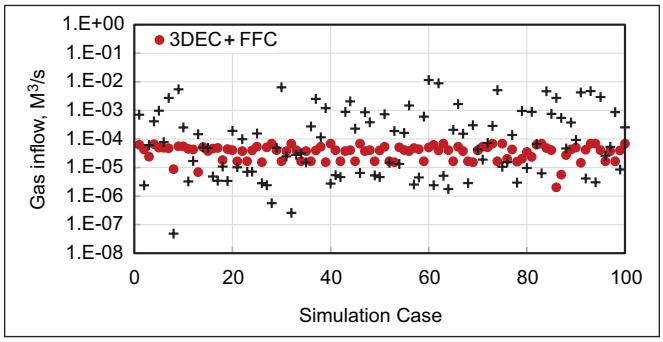

Figure 10. Comparison of inflow between 3DEC and FFC for a simple case of flow through a network of fractures with constant aperture values in 3DEC

set to be constant to save computational time but DFN geometries follow distributions discussed in section 2-2-1.

One hundred DFN realizations are run by 3DEC and FFC to model variation in the fracture geometry, and the results are compared in Figure 10. The results show an agreement between both models with a difference in the standard deviation of inflow values that can be related to the difference in the DFN treatment methods in 3DEC and FFC.

Inflow Estimation

As described in previous sections, the FFC model is used to predict potential flow to the mine in the event of a shale gas well casing breach. The spatial distribution of fracture apertures obtained by 3DEC (Figure 9) shows that the aperture of mining-induced fractures over the elastic regions towards the center of the pillar is different from the region over the gob or high-stressed zone towards the edge of the panel. Therefore, the FFC model is classified into three transport zones for each panel: headgate chain pillar area, gob area, and tailgate abutment pillar area (Figure 3).

The peak values of the lognormal distribution for each depth range are obtained from the 3DEC aperture results and are summarized in Table 2. The aperture values in Table 2 are assumed to be the hydraulic aperture, which means the entire width of the fracture opening is available for fluid flow ($F = 1$).

After the FFC model is set up, the calculated permeabilities at the Sewickley horizon are compared with the field measurement for validation. Figure 11 shows the comparison between the field measurements and the permeability for 100 realizations from the FFC model at the Sewickley horizon. The computed results are within one order of magnitude of the measured permeabilities, but due to the aperture grouping method in Table 2, the FFC overestimates the permeability values. Consequently, the estimated inflow in the FFC is expected to be conservative. More efficient techniques for importing the 3DEC aperture values will reduce the difference between measured and computed permeabilities in Figure 11.

The inflow to the mining area is estimated by assuming a breached point at the center of the abutment pillar at the Sewickley horizon (23 m above the mine level). Even though there could be several wells on a well pad, this study focuses on a single casing breach at the Sewickley horizon. One hundred stochastic DFN realizations are generated to model variation in the fracture geometry, connectivity, and aperture with each realization, representing a 1% probability of the overburden fracture network. Results are summarized in Table 3.

It is observed that predicted gas flow to the mine is higher for the second panel due to the enhancement in the mining-induced permeabilities during the completion of the second panel. For the first panel, there is about 91% probability that the gas flow to the mine is less than 0.05 m^3/s (100 cfm) and for the second panel a 37% probability that gas flow to the mine is less than 0.05 m^3/s (100 cfm). Out of the 100 realizations for the first panel mining, only one case of gas flow to the mine is predicted to be greater than 0.47 m^3/s (1,000 cfm). However, for the second panel, 11 out of the 100 realizations predicted a gas flow to the mine that is greater than 0.47 m^3/s (1,000 cfm).

This significant difference between first and second panels' gas inflow is related to the variation in the mining-induced permeability. The overall permeabilities of the area above the pillars are enhanced by the completion of the second panel. This is because of the

Table 2. Peak values of the lognormal distribution used for modeling vertical and horizontal fracture apertures in the FFC model

Depth (m)	Peak Values of the Lognormal Distribution for Fracture Aperture (mm)							
	Rib Area				Gob Area			
	Bedding Planes		Vertical Fractures		Bedding Planes		Vertical Fractures	
	First Panel	Second Panel	First Panel	Second Panel	First Panel	Second Panel	First Panel	Second Panel
0–15	0.1	0.1	0.1	0.1	0.1	0.1	0.1	0.1
15–30	0.1	0.1	0.1	0.2	0.01	0.2	0.3	0.3
30–40	0.1	0.4	0.3	0.5	0.6	0.8	0.1	0.1
40–45	0.4	0.7	0.6	0.8	0.9	1.0	1.0	2.0
45–70	0.1	0.3	0.2	0.4	0.2	0.3	0.6	0.7
70–90	0.2	0.4	0.2	0.5	0.3	0.4	0.5	0.7
90–110	0.3	0.4	0.4	0.5	0.4	0.5	0.7	0.8
110–130	0.4	0.6	0.6	0.9	0.5	0.7	0.8	1.5
130–135	0.6	0.9	0.7	1.5	0.8	0.9	2.0	3.0

Table 3. Summary of conservative inflow estimates from 100 DFN realizations for a single well casing breach at the Sewickley horizon

Gas Flow to the Mine m^3/s (cfm)	Number of Simulated Cases	
	First Panel	Second Panel
0 (0)–0.05 (100)	91	37
0.05 (100)–0.19 (400)	7	38
0.19 (400)–0.33 (700)	1	10
0.33 (700)–0.47 (1,000)	0	4
>0.47 (1,000)	1	11

increase in the volume of disturbed rock from the first to the second panel mining. The implication of the different flow rates to the mine conditions are a subject of an ongoing research at NIOSH but as discussed in the next section, the technique presented in this paper in its current form is useful for comparative analyses over different geology conditions and designs and not for obtaining absolute values of inflow.

DISCUSSION ON LIMITATIONS

It is important to note that the FFC is a 2D model with the assumption of a 1-m thickness in the out-of-plane direction; hence, the flow calculated is the total boundary flow per meter. This means we assume the out-of-plane length for both the breached area (pressure source) and the fracture network is one meter, while changing this value, especially for the breached area, can drastically change the results of the estimated inflow. Besides, the comparison in Figure 11 shows that the FCC overestimates the permeability values due to the simplified grouping method in Table 2, so it is expected that the inflow values in Table 3 are conservative. Therefore, the inflow for different realizations in this paper may be used for a comparative analysis and not for absolute values of potential inflow to the mine. Further analyses are required for a complete transfer of aperture values from 3DEC to FFC, analyzing effects of bedding planes on the overall permeability, and investigating the effects of out-of-plane length of the model on the inflow values.

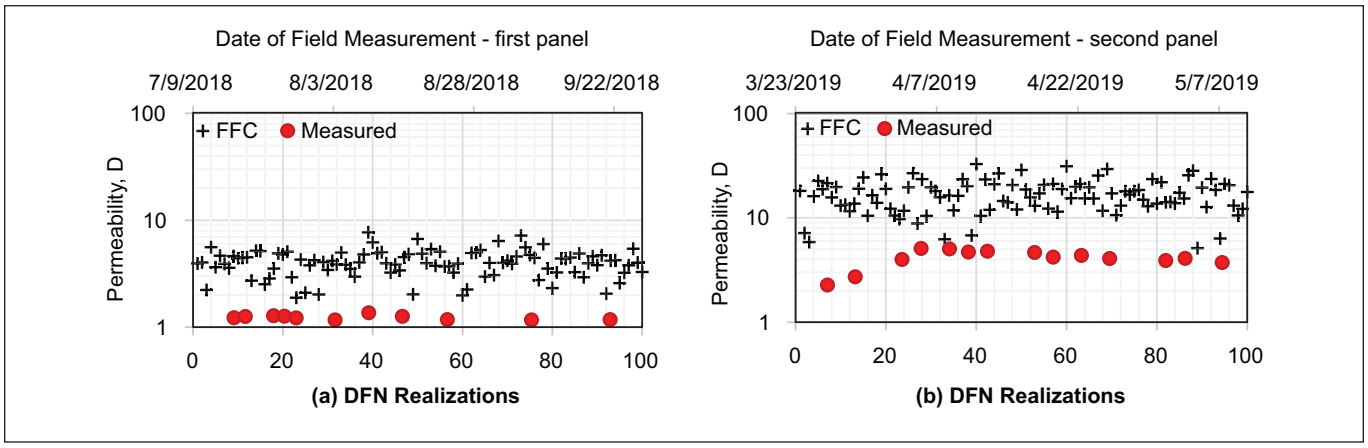

Figure 11. Comparison of permeabilities computed by FFC and measured at the Sewickley Horizon for (a) first panel and (b) second panel completion

CONCLUSION

A modeling methodology is presented in this paper for quantitative analyses of mining effects on the rockmass permeability and potential inflow to the mining area in case of a breached gas well in an abutment pillar. Surface and underground in-situ measurements in a shallow longwall mine are used to calibrate and then validate a pseudo-2D geomechanical model that extrapolates measured values and extends the understanding of mining-induced permeability during the completion of two longwall panels. The computed permeabilities across the two panels are grouped into six main areas and are imported to a 2D FFC model to stochastically analyze potential gas inflow to the mine in case of a gas well breach. An improvement to this methodology could be a fully detailed transfer of aperture values from the geomechanical model to the FFC. Results show that the gas inflow remains below 0.19 m^3/s in 98% and 75% of cases after the completion of first and second panels, respectively. In comparison, the inflow exceeds 0.47 m^3/s in 1% of cases after mining the first and in 11% of cases after the second panel is completed. It is important to note that the inflow estimates in this paper are useful for comparative analyses amongst different cases because calculating absolute values requires improvement on the 2D modeling assumptions, aperture grouping techniques, and modeling overall permeabilities. The presented numerical approach provides a tool for investigating the hazards associated with a gas well breach and evaluating the mitigation techniques.

DISCLAIMER

The findings and conclusions in this paper are those of the authors and do not necessarily represent the official position of the National Institute for Occupational Safety and Health, Centers for Disease Control and Prevention. Mention of any company or product does not constitute endorsement by NIOSH.

REFERENCES

Best, DJ, and Nicholas I Fisher. 1979. 'Efficient simulation of the von Mises distribution', *Applied Statistics*: 152-57.

Commonwealth of Pennsylvania, Department of Mines and Mineral Industries, Oil and Gas Division, Joint Coal and Gas Committee. 1957. "Gas Well Pillar Study." In, 28. Harrisburg, Pennsylvania.

aaFeng, Guorui, Zhen Li, Shengyong Hu, Yuting Zhang, Ao Zhang, Qiang Gao, Haina Jiang, Xiangqian Guo, Chao Li, and Jiaqing Cui. 2018. 'Distribution of gob empty space for methane drainage during the longwall mining: A case study', *Journal of Natural Gas Science and Engineering*, Volume 60: 112–24.

Holla, L., and M. Buizen. 1991. 'The ground movement, strata fracturing and changes in permeability due to deep longwall mining', *International Journal of Rock Mechanics and Mining Sciences & Geomechanics Abstracts*, 28: 207–17.

Iannacchione, A. T. 1990. "The Effects of Roof and Floor Interface Slip on Coal Pillar Behavior." In *31st US Symposium on Rock Mechanics.*

Kissell, Fred N, and John C Edwards. 1975. 'Two-phase flow in coalbeds'.

Kohl, W. R. 1980. "Jointing in outcropping rocks of Pennsylvanian age, central Greater Pittsburgh region, Pennsylvania." In. https://pubs.usgs.gov/of/1980/0023/report.pdf: U.S. Geological Survey.

PADEP. 2018. "2018 Oil and Gas Annual Report." In, edited by Pennsylvania Department of Environmental Protection.

Palchik, V. 2003. 'Formation of fractured zones in overburden due to longwall mining', *Environmental Geology*, 44: 28–38.

Su, D. W. H., P. Zhang, H. Dougherty, M. Van Dyke, T. Minoski, S. Schatzel, V. Gangrade, E. Watkins, J. Addis, and C. Hollerich. 2019. "Effects of Longwall-Induced Subsurface Deformations and Permeability Changes on Shale Gas Well Integrity and Safety Under Shallow Cover." In *53rd U.S. Rock Mechanics/ Geomechanics Symposium*.

Watkins, E., Gangrade, V., Schatzel, S.J., Karacan, C.O., Hollerich, C., Addis, J. 2020. "Permeability determination for potential interaction between shale gas wells and the coal mine environment due to longwall-induced deformations." In *Annual Conference of Society of Mining, Minerals, and Exploration*. Phoenix, AZ.

Zhang, Peter, Heather Dougherty, Daniel Su, Jack Trackemas, and Berk Tulu. 2020. 'Influence of longwall mining on the stability of gas wells in chain pillars', *International Journal of Mining Science and Technology*, 30: 3–9.

Zhang, X., D. J. Sanderson, R. M. Harkness, and N. C. Last. 1996. 'Evaluation of the 2-D permeability tensor for fractured rock masses', *International Journal of Rock Mechanics and Mining Sciences & Geomechanics Abstracts*, 33: 17–37.